Pyrolysis treatment of nonmetal fraction of waste printed circuit boards: Focusing on the fate of bromine

Pyrolysis treatment of nonmetal fraction of waste printed circuit boards: Focusing on the fate of bromine

Jingjing Xiong[1], Shaoqi Yu[1], Daidai Wu[2], Xiaoshu Lü[3,4,5], Junhong Tang[1], Weihong Wu[1] and Zhitong Yao[1]

Abstract

Advanced thermal treatment of electronic waste offers advantages of volume reduction and energy recovery. In this work, the pyrolysis behaviour of nonmetallic fractions of waste printed circuit boards was studied. The fate of a bromine and thermal decomposition pathway of nonmetallic fractions of waste printed circuit boards were further probed. The thermogravimetric analysis showed that the temperatures of maximum mass loss were located at 319°C and 361°C, with mass loss of 29.6% and 50.6%, respectively. The Fourier transform infrared Spectroscopy analysis revealed that the spectra at temperatures of 300°C–400°C were complicated with larger absorbance intensity. The nonmetallic fractions of waste printed circuit boards decomposed drastically and more evolved products were detected in the temperature range of 600°C–1000°C. The gas chromatography–mass spectrometry analysis indicated that various brominated derivates were generated in addition to small molecules, such as CH_4, H_2O and CO. The release intensity of CH_4 and H_2O increased with temperature increasing and reached maximum at 600°C–800°C and 400°C–600°C. More bromoethane (C_2H_5Br)was formed as compared with HBr and methyl bromide (CH_3Br). The release intensity of bromopropane (C_3H_7Br) and bromoacetone (C_3H_5BrO) were comparable, although smaller than that of bromopropene (C_3H_5Br). More dibromophenol ($C_6H_4Br_2O$) was released than that of bromophenol (C_6H_5BrO) in the thermal treatment. During the thermal process, part of the ether bonds first ruptured forming bisphenol A, propyl alcohol and tetrabromobisphenol A. Then, the tetrabromobisphenol A decomposed into C_6H_5BrO and HBr, which further reacted with small molecules forming brominated derivates. It implied debromination of raw nonmetallic fractions of waste printed circuit boards or pyrolysis products should be applied for its environmentally sound treating.

Keywords

Electronic waste, waste printed circuit boards, brominated flame retardant, flame retardant plastics, pyrolysis

Introduction

The rapid innovations rate and replacement frequency of electrical and electronic equipment has resulted in shorter and shorter lifespans for these products (Li et al., 2015; Yao et al., 2018; Zeng et al., 2018). The waste from end-of-life electrical and electronic equipment, known as electronic waste (e-waste), has become the world's fastest growing waste problem (Wang et al., 2016; Yao et al., 2019a; Yao et al., 2019b). The recent report from United Nations University 'Global E-waste Monitor 2017: Quantities, Flows, and Resources' (Baldé et al., 2017) reported that, 44.7 million metric tonnes of e-waste was generated worldwide in 2016 and will reach 52.2 million metric tonnes by 2021. According to the report 'White paper on WEEE recycling industry in China 2017' (CHEARI, 2018), the theoretical amount of scrapped residential equipment in 2017 reached 1.25 billion units, including 32.16 million television sets, 24.39 million refrigerators, 16.20 million washing machines, 27.23 million air conditioners and 25.24 million personal computers. Duan et al. (2016) reported that approximately 1.8 million tonnes of e-waste will be generated by 2020.

Printed circuit boards (PCB) are a major and critical constituent of electrical and electronic equipment and the resulted waste PCB (WPCB) accounts for approximately 3–6 wt.% of the total e-waste (Kumar et al., 2018a; Premur et al., 2016). The WPCB generally contains 10 wt.% of copper, 1000 ppm of silver and 200 ppm of gold, 10 times higher than that in natural ores. Recently, recovering valuable metals from WPCB has

[1]College of Materials and Environmental Engineering, Hangzhou Dianzi University, Hangzhou, China
[2]Chinese Academy of Sciences, Guangzhou Institute of Energy Conversion, Guangzhou, China
[3]Department of Electrical Engineering and Energy Technology, University of Vaasa, Vaasa, Finland
[4]Department of Civil Engineering, Aalto University, Espoo, Finland
[5]Construction Engineering College, Jilin University, Chang Chun, China

drawn more attention and has become one of the most profita- ble business in the recycling industry. To facilitate the WPCB recycling, many sophisticated technologies had been devel- oped, including mechanical–physical approach (Nekouei et al., 2018), pyrometallurgy (Wang et al., 2017a), hydrometallurgy(Li et al., 2018), biometallurgy (Kumar et al., 2018b), electroly- sis (Yang et al., 2018a) and supercritical fluid (Xiu et al., 2017).Among them, the mechanical–physical process has been proven to be technologically feasible, and widely used in e-waste recy- cling plants worldwide (Guo et al., 2014). During this process, metallic and nonmetallic fractions of WPCB (NMF–WPCB) are separated by coupled mechanical separations, such as electrostatic separation, pneumatic separation and eddy current separation. NMF–WPCB accounts for 60–70 wt.% of WPCB and has hybrid components of brominated resins, glass fibre and ceramic materials, which pose a major challenge to the environment (Chen et al., 2018). Recently, explorative researches using NMF–WPCB to prepare polymer composites (Hu et al., 2018; Kovačević et al., 2017), building materials (Kurup and Senthil Kumar, 2017; Xin et al., 2017) and absor- bents (Hadi et al., 2015; Xu et al., 2014) have been conducted. However, the utilisation rate is low, and there is still a long way to go to achieve large-scale application.

Advanced thermal treatment offers advantages of significant volume reduction and energy recovery (Cheng et al., 2019; Muhammad et al., 2015; Qi et al., 2019; Yu et al., 2019). The study on thermal decomposition behaviour of NMF–WPCB is significant and has been reported in some literatures. Long et al. (2010) developed the vacuum pyrolysis of NMF–WPCB and analysed the products and residues. Cai et al. (2018) investigated the emission characteristics of polycyclic aromatic hydrocarbons during WPCB pyrolysis. De Marco et al. (2008) conducted the pyrolysis of WPCB to recover metals, energy or chemicals. However, the decomposition mechanism and pathway for the thermal treatment of NMF–WPCB was not sufficient to support its industrial recycling. Therefore, we investigated not only the pyrolysis behaviours of NMF–WPCB, but also the fate of the brominated flame retardant and thermal decomposition pathway. Our results will offer practical support for the thermal treatment of halogen-containing wastes, such as polyurethane foam from waste refrigerators, television plastic shells and polyvinyl chloride plastics.

Materials and methods

Materials

The FR4 WPCBs were collected from a typical large-scale electrical and electronic equipment recycling plant located in Linyi, China. They were first underwent a two-step crushing, followed by magnetic separation and electrostatic separation, and then the NMF–WPCB was obtained. The samples were sieved and particles with size of 0.32–0.63 mm were collected. The major chemical compositions of NMF–WPCB were determined using inductively coupled plasma optical emission spectroscopy (ICP–OES, Optima 8000, Perkin Elmer) after digested by a HNO_3-HF-H_2O_2 system. It consisted of the following elements (in wt.%): carbon 49.9, oxygen 15.4, silicon 9.2, bromine 8.6, calcium 6.3, aluminium 3.5, copper 2.8 , iron 0.6 and magnesium 0.5.

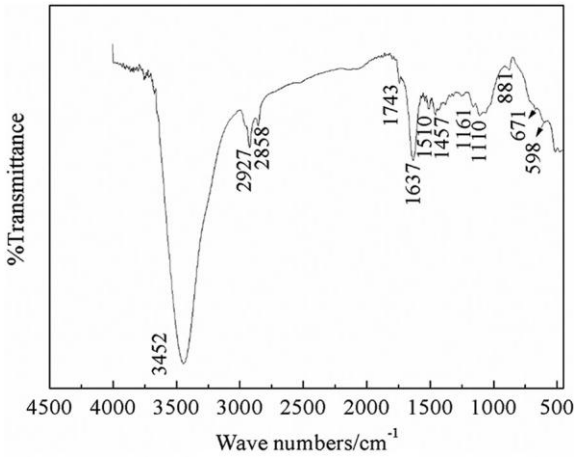

Figure 1. FT–IR spectrum of NMF–WPCB sample.

Experimental

The Fourier transform infrared (FT-IR) analysis of the NMF–WPCB sample was conducted by a NEXUS 670 FT-IR spectrometer (Thermo Nicolet Corporation). Online testing of evolved products during the NMF–WPCB pyrolysis was performed using a thermogravimetric-gas chromatography-mass spectrometry coupled with a Fourier transform infrared spectrometer (TG-FTIR-GC/MS) coupled system (TGIRGCMS*/TGA8000*, Perkin Elmer). During analysis, approximately 2 mg of samples were heated from 20°C to 1000°C at a selected heating rate of 20°C min^{-1} with helium flowrate of 50 mL min^{-1}. Each test was repeated at least three times. The coupling systems between the TG-FTIR-GC/MS were heated to 280°C, preventing the condensation of volatile products.

Results and discussion

Characterisation of NMF-WPCB

The FTIR spectrum of NMF–WPCB sample is displayed in Figure 1. Bands at 3452 and 1637 cm^{-1} corresponded to the O–H stretching and bending vibrations (Cui et al., 2011; Du et al., 2018). Peaks located at 2927 and 2858 cm^{-1} confirmed the antisymmetric and symmetric C–H vibration (Hu et al., 2011). The band at 1743 cm^{-1} was associated with the C=O stretching (Bao et al., 2015; Pornsunthorntawee et al., 2008). Bands at 1510, 1457, 1161 and 1110 cm^{-1} originated from the C=C stretching of the aromatic ring (Khattri and Singh, 2009), -CH_2 bending and C–O stretching (Yin et al., 2007), respectively. Minor peaks at 881, 598 and 671 cm^{-1} were ascribed to the asymmetric Si–O stretching (Niu et al., 2013), Si–O bending (Michalski et al., 2003) and C–Br group (Hu et al., 2017; Wang et al., 2017b), respectively. These peaks were well consistent with the brominated bisphenol A epoxy resins present in FR4 PCB (Zhao et al., 2017).

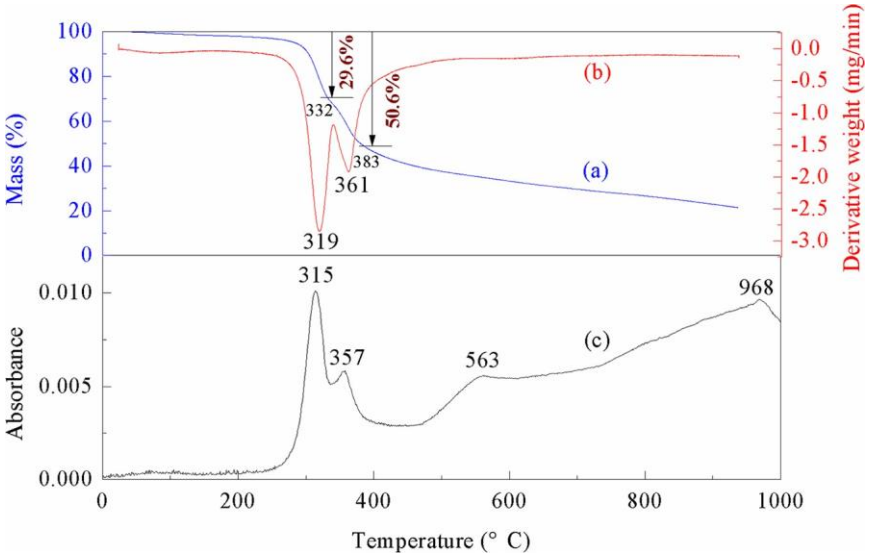

Figure 2. TG–DTG and RMS intensity profiles of NMF–WPCB pyrolysis.

Thermogravimetric analysis

The thermogravimetric (TG) curve (see Figure 2(a)), derivative thermogravimetric (DTG) curve (see Figure 2(b)) and root mean square (RMS) (see Figure 2(c)) intensity profiles of the NMF–WPCB are illustrated in Figure 2. The TG curve indicates that its thermal decomposition showed a three-stage process with two significant mass loss rates in the temperature ranges of 20°C–332°C and 332°C–383°C. The mass loss was determined as 29.6%, 21.0% and 28.0% for these stages, respectively. The DTG curve indicated that the temperatures of maximum mass loss rate were located at 319°C and 361°C with a corresponding mass loss of 29.6% and 50.6%. This was consistent with literature (Rajagopal et al., 2017), where it was reported that the polymeric content of WPCB underwent major decomposition at 300°C. During the first decomposition stage, part of ether bonds in the brominated resin ruptured into bisphenol A, propyl alcohol and tetrabromobisphenol A (Shin et al., 2019). In addition, the epoxy group ruptured resulting in the release of small molecules. The weight loss in the second stage was attributed to the decomposition of tetrabromobisphenol A (Evangelopoulos et al., 2015). In the third stage, most organics decomposed forming small molecules. The detected peaks of the RMS or Gram–Schmidt (GS) intensity profiles of the total evolved gases were successfully used in the FT-IR experiment in parallel with the TG curves (Paama et al., 2003, Suuronen et al., 2002). The RMS profile indicated that the major decomposition of NMF–WPCB occurred at 315°C and 968°C. The RMS intensity increased non-significantly at a temperature above 357°C, indicating a smaller decomposition rate at later stages.

FT-IR analysis

Three-dimensional (3D) FT-IR spectra of the gas phase during the thermal decomposition of NMF–WPCB are displayed in Figure 3. In view of the *Y*-axis (temperature) and *Z*-axis

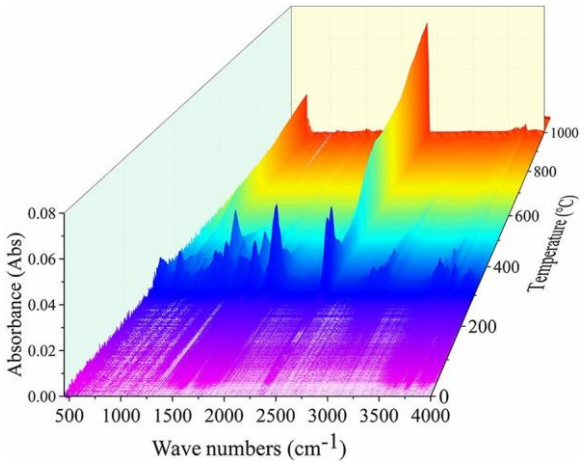

Figure 3. 3D infrared spectrum of the evolved products for NMF–WPCB pyrolysis.

(absorbance), the NMF–WPCB decomposed drastically and the release intensity of evolved gas product was significant throughout the temperature range of 600°C–1000°C. This was consistent with the RMS intensity profile in Figure 2. From the perspective of the *X*-axis (wavenumbers) and *Y*-axis (temperature), weak absorbance was observed at a temperature of 20°C–300°C. In addition, it was not distinct in the spectra shape at 600°C–1000°C. The spectra at 300°C–400°C was complicated (which will be confirmed later) with larger absorbance intensity. From the point of the *X*-axis (wavenumbers) and *Z*-axis (absorbance), the absorbance peaks were mainly located at 670, 1175, 1509, 1743, 2311 and 2358 cm^{-1} (confirmed in Figure 4).

Major signals from the gas-phase spectra were further separated from the 3D spectra (Figure 5) according to the 2D spectra and DTG results. Major peaks concentrated at 670, 2310, 2358 and 3734 cm^{-1} were attributed to the bending modes, asymmetric stretching mode and combination bands of CO_2 (Petkova et al., 2005; Xie and Pan, 2001), respectively. At 253°C, the absorbance

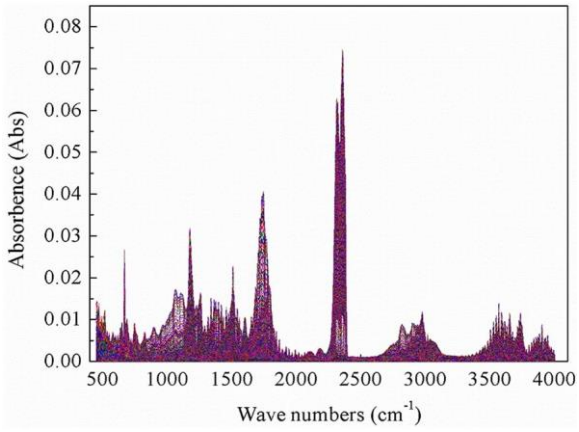

Figure 4. 2D infrared spectrum of the evolved products for NMF–WPCB pyrolysis.

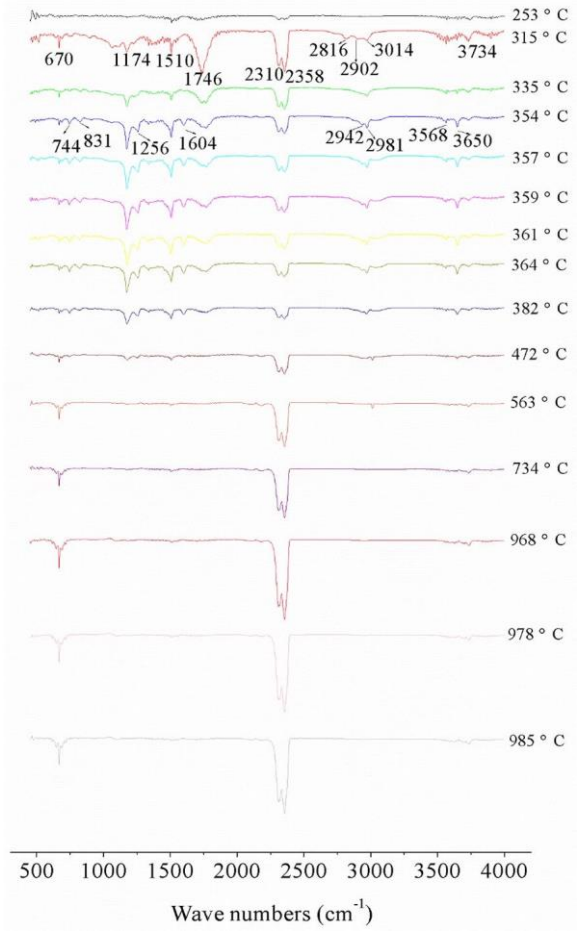

Figure 5. FTIR spectra of volatilised products in NMF–WPCB pyrolysis.

intensity was relatively weak. Except for the absorbance of CO_2, a weak peak located at 1510 cm^{-1} could be detected, which was ascribed to the aromatic ring stretching vibration (Gu et al., 2009). The weight loss of NMF-WPCB was calculated as 3.13% throughout the temperature 20°C–253°C, indicating that most bonds had not begun to break at this stage. At 315°C, the spectrum became complicated. The release intensity of CO_2 increased significantly and new peaks were detected. Absorbance at 1174 and 1746 cm^{-1} were attributed to the epoxy group (Lee et al., 2016) and ester carbonyl stretching mode (Mac Aleese et al., 2006). Weak peaks at 2816, 2902 and 3014 cm^{-1} were owing to the asymmetric C–H stretching and asymmetric -CH_3 stretching, respectively. At 354°C, the release intensity of CO_2 and ester carbonyl at 1746 cm^{-1} decreased at the expense of new peaks forming. Peaks at 744 and 831 cm^{-1} corresponded to the C–Br stretching (Giraud et al., 2009) and C=CH- out-of-plane bending vibration (Worzakowska and Ścigalski, 2013), indicating the decomposition of brominated resin. Peaks located at 1256 and 1604 cm^{-1} were ascribed to the symmetric -CH_3 bending vibration and C–C stretching in the benzene ring (Yang et al., 2018b). A set of bands at 2816, 2902 and 3014 cm^{-1} disappeared and new peaks at 2942 and 2981 cm^{-1} owing to aliphatic C–H stretching vibration were observed (Kleindienst et al., 2002), further confirming the decomposition of polymer moleculars. In addition, new peaks located at 3568 and 3650 cm^{-1} were detected, which could be assigned to the hydroxyl on the aromatic ring of grafted phenol (Kandziolka et al., 2014; Ma et al., 2017). With temperatures increasing to 357°C–472°C, most peaks decreased significantly except the absorbance of CO_2. Further increasing temperatures to 563°C–985°C, the absorbance at 2981 cm^{-1} decreased continuously, whereas, the release intensity of CO_2 increased.

Gas chromatography–mass spectrometry(GC–MS) analysis

Mass spectrum of evolved products with mass-to-charge ratio (m/z) from 12 to 252 were analysed and displayed in Figure 6. Signals from m/z 12, 16 and 18 presented the evolution of small molecules CO, CH_4 and H_2O, respectively. The release of CO was mainly focused at 500°C above. The release intensity of CH_4 and H_2O increased with increasing temperature and reached maximum intensity at 600°C–800°C and 400°C– 600°C. In addition, more CH_4 and H_2O were released as com- pared with CO. Ion signals from m/z 81, 93 and 108 presented the evolution of hydrogen bromide (HBr), methyl bromide (CH_3Br) and bromoethane (C_2H_5Br), the intensity of which increased with an increase of temperature. The maximum releasing rate was observed at 545°C, 597°C and 673°C, respec- tively. More C_2H_5Br were generated than HBr and CH_3Br. Signals with m/z 121, 123 and 137 were attributed to the bromo-propene (C_3H_5Br), bromopropane (C_3H_7Br) and bromoacetone (C_3H_5BrO). Their release increased with raising temperature and reached the peak at approximately 650°C. The release intensity of C_3H_7Br and C_3H_5BrO were similar, although smaller than that of C_3H_5Br. Iron signals with m/z 173 and 252 were ascribed to the bromophenol (C_6H_5BrO) and dibromophe- nol ($C_6H_4Br_2O$) evolution, whose release intensity increased with elevating temperature and reached maximum intensity at 600°C–700°C and 400°C–600°C. More $C_6H_4Br_2O$ was gener- ated than that of C_6H_5BrO in whole thermal process.

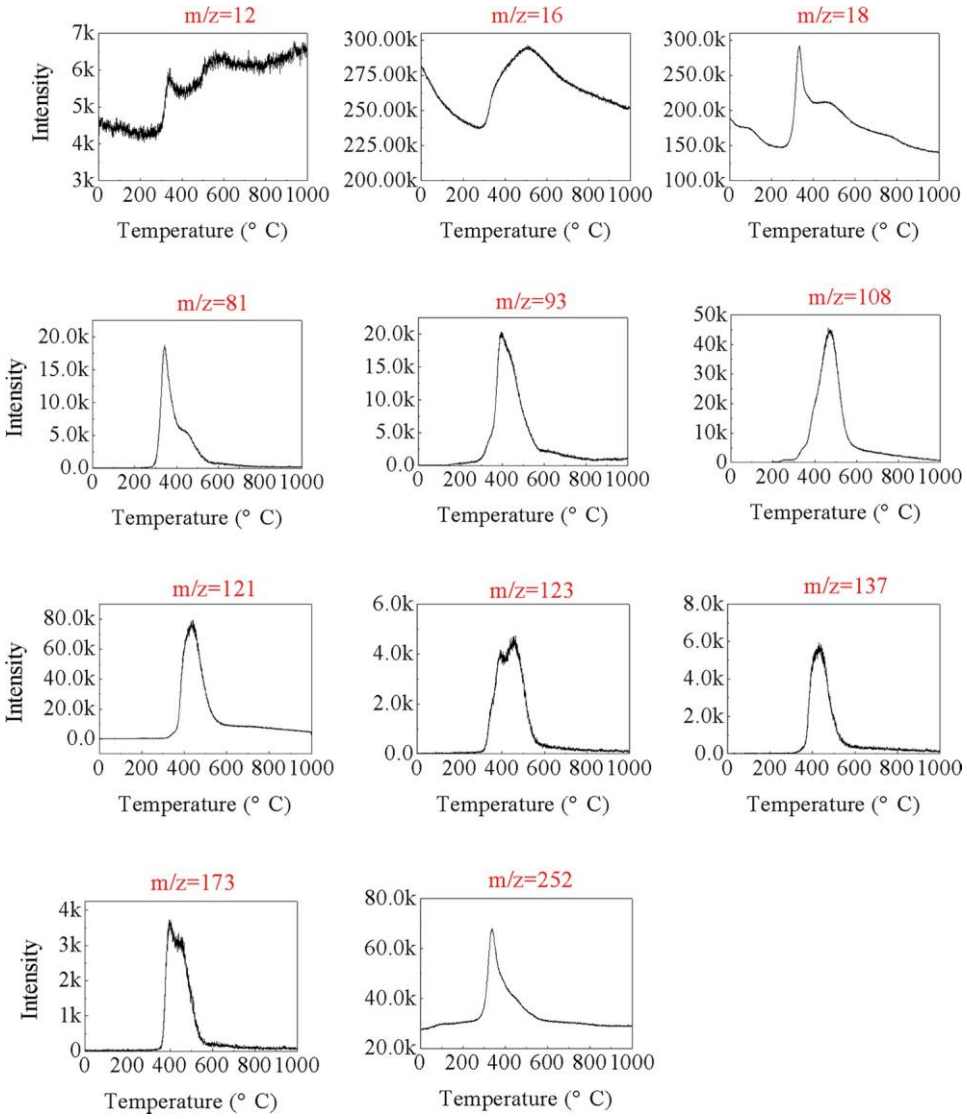

Figure 6. Mass spectra of the evolved products in NMF–WPCB pyrolysis.

Decomposition pathway

Based on the above analysis, the decomposition pathway of NMF–WPCB is illustrated in Figure 7. The whole decomposition process cab be divided into three stages. First, part of the ether bonds in the brominated resin ruptured at less than 335°C, forming three major evolved products – bisphenol A, propyl alcohol and tetrabromobisphenol A. This was consistent withthe literature (Evangelopoulos et al., 2015; Luda et al., 2002). The epoxy group was also broken resulting in the release ofCO_2, which can be confirmed by the FT-IR result in Figure 5. Second, the tetrabromobisphenol A decomposed into C_6H_5BrO and HBr, which further reacted with small molecules (degrada- tion of bisphenol A and propyl alcohol) forming brominated products, such as CH_3Br, C_2H_5Br, C_3H_5Br and C_3H_7Br. In this stage, small molecules H_2O, CO and CO_2 were also generated. The release intensity of C_2H_5Br, C_3H_5Br, C_6H_5BrO, $C_6H_4Br_2O$, CO_2 and H_2O were larger as compared with that of others. At the last stage, most organics were decomposed forming CH_4, CO and CO_2, which can also be confirm by the FT-IR result in Figure 5. This implied the debromination of raw NMF–WPCB or pyrolysis products should be conducted for environmentally sound treating and effective energy recovering from this waste. Recently, some preliminary experiments have been reported. Gao and Xu (2019) added $CaCO_3$ during the pyrolysis of NMF–WPCB and the bromine was fixed as $CaBr_2$. Shen (Shen, 2018; Shen et al., 2018) applied alkali (e.g. NaOH, KOH) to treat NMF–WPCB before pyrolysis, improving the bromine fixation in the solid char.

Conclusions

The TG analysis indicated that there were two significant weight loss events throughout the temperature ranges of 20°C–332°C and 332°C–383°C. The temperature of maximum mass loss rate was determined as 319°C and 361°C. The FT-IR analysis revealed that the NMF–WPCB decomposed vigorously and more gaseous products were released at temperature of 600°C–1000°C. The spectra at temperate of 300°C–400°C was complicated with larger absorbance intensity. The GC-MS analysis illustrated that the release intensity of

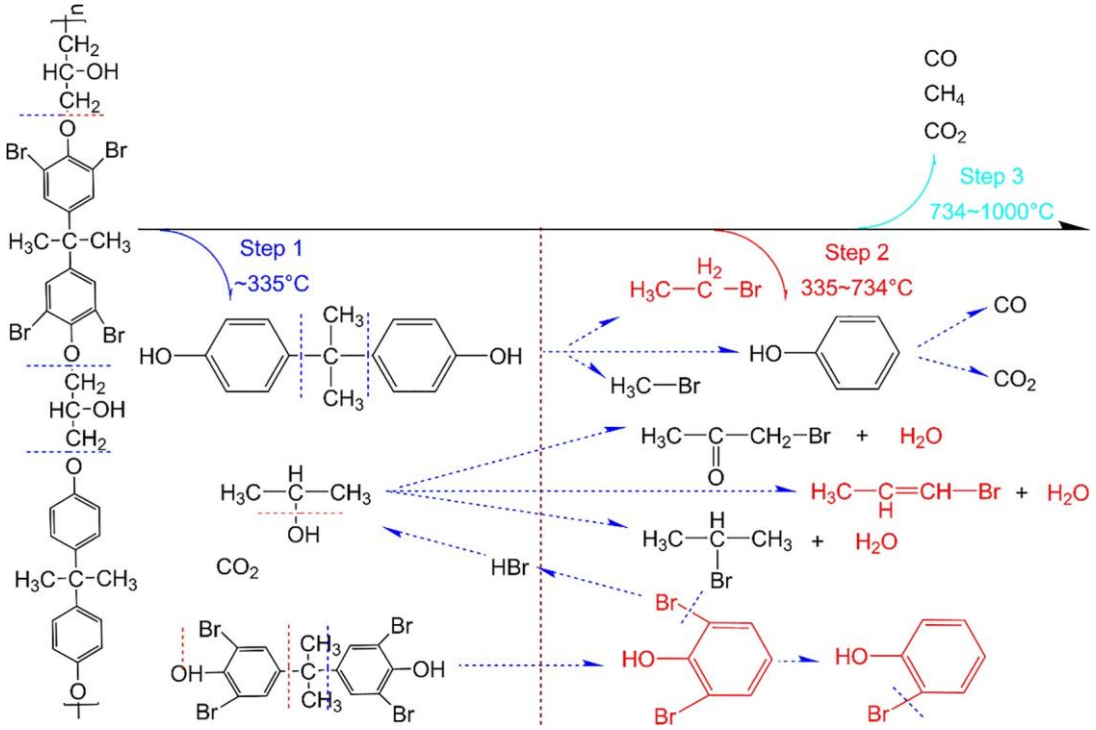

Figure 7. Thermal decomposition mechanism for NMF–WPCB pyrolysis.

CH_4 and H_2O increased with increasing temperature and reached maximum at temperatures of 600°C–800°C and 400°C–600°C. The release intensity of C_3H_7Br and C_3H_5BrO were comparable although smaller than that of C_3H_5Br. More $C_6H_4Br_2O$ was generated compared with that of C_6H_5BrO in the whole decomposition process. Regarding the decomposition process, part of the ether bonds first ruptured into bisphenol A, propyl alcohol and tetrabromobisphenol A. Then, the tetrabromobisphenol A decomposed into C_6H_5BrO and HBr, which further reacted with small molecules forming brominated products. At the last stage, most organics decomposed forming small molecules, such as CH_4, CO and CO_2.

Declaration of conflicting interests

The authors declared no potential conflicts of interest with respect to the research, authorship, and/or publication of this article.

Funding

The authors disclosed receipt of the following financial support for the research, authorship, and/or publication of this article: This work was financially supported by the National Natural Science Foundation of China [Grant no. 21911530766, 51911530460 and 51606055] and Zhejiang Provincial Natural Science Foundation of China [Grant no. LY19B070008].

ORCID iD

Zhitong Yao https://orcid.org/0000-0002-9180-2329

References

Baldé CP, Forti V, Gray V, et al. (2017) *The global e-waste monitor 2017: Quantities, flows and resources*. United Nations University, International Telecommunication Union, and International Solid Waste Association.

Bao L, Liu C, Zhang ZL, et al. (2015) Photoluminescence-tunable carbon nanodots: Surface-state energy-gap tuning. *Advanced Materials* 27: 1663–1667.

Cai C, Yu S, Li X, et al. (2018) Emission characteristics of polycyclic aromatic hydrocarbons from pyrolytic processing during dismantling of electronic wastes. *Journal of Hazardous Materials* 351: 270–276.

CHEARI (2018) White Paper on Chinese WEEE Recycling Industry in China (2017). Beijing (in Chinese).

Chen Y, Zhang Y, Yang J, et al. (2018) Improving bromine fixation in co-pyrolysis of non-metallic fractions of waste printed circuit boards with Bayer red mud. *Science of The Total Environment* 639: 1553–1559.

Cheng S, Qiao Y, Huang J, et al. (2019) Effects of Ca and Na acetates on nitrogen transformation during sewage sludge pyrolysis. *Proceedings of the Combustion Institute* 37: 2715–2722.

Cui S, Liu Y, Fan M, et al. (2011) Temperature dependent microstructure of MTES modified hydrophobic silica aerogels. *Materials Letters* 65: 606–609.

De Marco I, Caballero BM, Chomón MJ, et al. (2008) Pyrolysis of electrical and electronic wastes. *Journal of Analytical and Applied Pyrolysis* 82: 179–183.

Du W, Pu X, Sun J, et al. (2018) Synthesis and evaluation of a novel monomeric amine as sodium montmorillonite swelling inhibitor. *Adsorption Science & Technology* 36: 655–668.

Duan H, Hu J, Tan Q, et al. (2016) Systematic characterization of genera- tion and management of e-waste in China. *Environmental Science and Pollution Research* 23: 1929–1943.

Evangelopoulos P, Kantarelis E and Yang W (2015) Investigation of the thermal decomposition of printed circuit boards (PCBs) via thermogravimetric analysis (TGA) and analytical pyrolysis (Py-GC/MS). *Journal of Analytical and Applied Pyrolysis* 115: 337–343.

Gao R and Xu Z (2019) Pyrolysis and utilization of nonmetal materials in waste printed circuit boards: Debromination pyrolysis, temperature-controlled condensation, and synthesis of oil-based resin. *Journal of Hazardous Materials* 364: 1–10.

Giraud F, Loge C, Pagniez F, et al. (2009) Design, synthesis and evaluation of 3-(imidazol-1-ylmethyl) indoles as antileishmanial agents. Part II. *Journal of Enzyme Inhibition and Medicinal Chemistry* 24: 1067–1075.

Gu X, Sung L, Kidah B, et al. (2009) Multiscale physical characterization of an outdoor-exposed polymeric coating system. *Journal of Coatings Technology and Research* 6: 67–79.

Guo J, Fang W, Yang Y, et al. (2014) Effects of acoustic hood on noise, CFC-11, and particulate matter in a recycling system for waste refrigera-tor cabinet. *Environmental Science and Pollution Research* 21: 12701–12708.

Hadi P, Ning C, Ouyang W, et al. (2015) Toward environmentally-benign utilization of nonmetallic fraction of waste printed circuit boards as modifier and precursor. *Waste Management* 35: 236–246.

Hu D, Jia Z, Li J, et al. (2018) Characterization of waste printed circuit boards nonmetals and its reutilization as reinforcing filler in unsaturated polyester resin. *Journal of Polymers and the Environment* 26: 1311–1319.

Hu N, Meng L, Gao R, et al. (2011) A facile route for the large scale fabrication of graphene oxide papers and their mechanical enhancement by cross-linking with glutaraldehyde. *Nano-Micro Letters* 3: 215–222.

Hu Z, Shao Q, Moloney MG, et al. (2017) Nondestructive functionalization of graphene by surface-initiated atom transfer radical polymerization: An ideal nanofiller for poly (p-phenylene benzobisoxazole) fibers. *Macromolecules* 50: 1422–1429.

Kandziolka MV, Kidder MK, Gill L, et al. (2014) Aromatic–hydroxyl interaction of an alpha-aryl ether lignin model-compound on SBA-15, present at pyrolysis temperatures. *Physical Chemistry Chemical Physics* 16: 24188–24193.

Khattri SD and Singh MK (2009) Removal of malachite green from dye wastewater using neem sawdust by adsorption. *Journal of Hazardous Materials* 167: 1089–1094.

Kleindienst TE, Corse EW, Li W, et al. (2002) Secondary organic aerosol formation from the irradiation of simulated automobile exhaust. *Journal of the Air & Waste Management Association* 52: 259–272.

Kovačević T, Rusmirović J, Tomić N, et al. (2017) New composites based on waste PET and non-metallic fraction from waste printed circuit boards: Mechanical and thermal properties. *Composites Part B: Engineering* 127: 1–14.

Kumar A, Holuszko ME and Janke T (2018a) Characterization of the nonmetal fraction of the processed waste printed circuit boards. *Waste Management* 75: 94–102.

Kumar A, Saini HS and Kumar S (2018b) Bioleaching of gold and silver from waste printed circuit boards by Pseudomonas balearica SAE1 isolated from an e-waste recycling facility. *Current Microbiology* 75: 194–201.

Kurup AR and Senthil Kumar K (2017) Effect of recycled PVC fibers from electronic waste and silica powder on shear strength of concrete. *Journal of Hazardous, Toxic, and Radioactive Waste* 21: 06017001.

Lee B, Li K, Yoon HS, et al. (2016) Membrane of functionalized reduced graphene oxide nanoplates with angstrom-level channels. *Scientific Reports* 6: 28052.

Li H, Eksteen J and Oraby E (2018) Hydrometallurgical recovery of metals from waste printed circuit boards (WPCBs): Current status and perspectives–A review. *Resources, Conservation and Recycling* 139: 122–139.

Li J, Zeng X, Chen M, et al. (2015) "Control-Alt-Delete": Rebooting solutions for the e-waste problem. *Environmental Science & Technology* 49: 7095–7108.

Long L, Sun S, Zhong S, et al. (2010) Using vacuum pyrolysis and mechanical processing for recycling waste printed circuit boards. *Journal of Hazardous Materials* 177: 626–632.

Luda MP, Balabanovich AI and Camino G (2002) Thermal decomposition of fire retardant brominated epoxy resins. *Journal of Analytical and Applied Pyrolysis* 65: 25–40.

Ma Y, Wang J and Zhang Y (2017) TG-FTIR study on pyrolysis of waste printing paper. *Journal of Thermal Analysis and Calorimetry* 129: 1225–1232.

Mac Aleese L, Simon A, McMahon TB, et al. (2006) Mid-IR spectroscopy of protonated leucine methyl ester performed with an FTICR or a Paul type ion-trap. *International Journal of Mass Spectrometry* 249: 14–20.

Michalski JR, Kraft MD, Diedrich T, et al. (2003) Thermal emission spectroscopy of the silica polymorphs and considerations for remote sensing of Mars. *Geophysical Research Letters* 30: PLA2-1–PLA2-4.

Muhammad C, Onwudili JA and Williams PT (2015) Thermal degradation of real-world waste plastics and simulated mixed plastics in a two-stage pyrolysis-catalysis reactor for fuel production. *Energy & Fuels* 29: 2601–2609.

Nekouei RK, Pahlevani F, Rajarao R, et al. (2018) Two-step pre-processing enrichment of waste printed circuit boards: Mechanical milling and physical separation. *Journal of Cleaner Production* 184: 1113–1124.

Niu F, Liu J, Tao L, et al. (2013) Nitrogen and silica co-doped graphene nanosheets for NO 2 gas sensing. *Journal of Materials Chemistry A* 1: 6130–6133.

Paama L, Pitkänen I, Halttunen H, et al. (2003) Infrared evolved gas analysis during thermal investigation of lanthanum, europium and samarium carbonates. *Thermochimica Acta* 403: 197–206.

Petkova V, Pelovski Y, Dombalov I, et al. (2005) Thermochemical investigations of natural phosphate with ammonium sulfate additive. *Journal of Thermal Analysis and Calorimetry* 80: 701–708.

Pornsunthorntawee O, Wongpanit P, Chavadej S, et al. (2008) Structural and physicochemical characterization of crude biosurfactant produced by Pseudomonas aeruginosa SP4 isolated from petroleum-contaminated soil. *Bioresource Technology* 99: 1589–1595.

Premur V, Anić Vučinić A, Vujević D, et al. (2016) The possibility for environmental friendly recycling of printed circuit boards. *Journal of Sustainable Development of Energy, Water and Environment Systems* 4: 14–22.

Qi W, Liu G, He C, et al. (2019) An efficient magnetic carbon-based solid acid treatment for corncob saccharification with high selectivity for xylose and enhanced enzymatic digestibility. *Green Chemistry* 21: 1292–1304.

Rajagopal RR, Rajarao R, Cholake ST, et al. (2017) Sustainable composite panels from non-metallic waste printed circuit boards and automotive plastics. *Journal of Cleaner Production* 144: 470–481.

Shen Y (2018) Effect of chemical pretreatment on pyrolysis of non-metallic fraction recycled from waste printed circuit boards. *Waste Management* 76: 537–543.

Shen Y, Chen X, Ge X, et al. (2018) Thermochemical treatment of non-metallic residues from waste printed circuit board: Pyrolysis vs. combustion. *Journal of Cleaner Production* 176: 1045–1053.

Shin S, Mai VD and Lee D (2019) Chemical recycling of used printed circuit board scraps: Recovery and utilization of organic products. *Processes* 7: 22.

Suuronen J, Pitkänen I, Halttunen H, et al. (2002) Formation of the main gas compounds during thermal analysis and pyrolysis: Betaine and betaine monohydrate. *Journal of Thermal Analysis and Calorimetry* 69: 359–369.

Wang H, Zhang S, Li B, et al. (2017a) Recovery of waste printed circuit boards through pyrometallurgical processing: A review. *Resources, Conservation and Recycling* 126: 209–218.

Wang P, Chen S, Cao Z, et al. (2017b) NIR light-, temperature-, ph-, and redox-responsive polymer-modified reduced graphene oxide/mesoporous silica sandwich-like nanocomposites for controlled release. *ACS Applied Materials & Interfaces* 9: 29055–29062.

Wang Z, Zhang B and Guan D (2016) Take responsibility for electronic-waste disposal. *Nature News* 536: 23.

Worzakowska M and Ścigalski P (2013) TG/DSC/FTIR characterization of linear geranyl diesters. *Journal of Thermal Analysis and Calorimetry* 113: 53–60.

Xie W and Pan W (2001) Thermal characterization of materials using evolved gas analysis. *Journal of Thermal Analysis and Calorimetry* 65: 669–685.

Xin Y, Fuqiang D, Xingmin L, et al. (2017) Rheological properties and microstructure of printed circuit boards modified asphalt. *China Petroleum Processing & Petrochemical Technology* 19: 72–80.

Xiu F, Weng H, Qi Y, et al. (2017) A novel recovery method of copper from waste printed circuit boards by supercritical methanol process: Preparation of ultrafine copper materials. *Waste Management* 60: 643–651.

Xu M, Hadi P, Chen G, et al. (2014) Removal of cadmium ions from wastewater using innovative electronic waste-derived material. *Journal of Hazardous Materials* 273: 118–123.

Yang D, Chu Y, Wang J, et al. (2018a) Completely separating metals and nonmetals from waste printed circuit boards by slurry electrolysis. *Separation and Purification Technology* 205: 302–307.

Yang J, Pu Y, Miao D, et al. (2018b) Fabrication of durably superhydrophobic cotton fabrics by atmospheric pressure plasma treatment with a siloxane precursor. *Polymers* 10: 460.

Yao Z, Ling T, Sarker PK, et al. (2018) Recycling difficult-to-treat e-waste cathode-ray-tube glass as construction and building materi- als: A critical review. *Renewable and Sustainable Energy Reviews* 81: 595–604.

Yao Z, Yu S, Su W, et al. (2019a) Kinetic modeling study on the com- bustion treatment of cathode from spent lithium-ion batteries. *Waste Management & Research*. Epub ahead of print 11 October 2019. DOI: 10.1177/0734242X19879224.

Yao Z, Yu S, Su W, et al. (2019b) Comparative study on the pyrolysis kinetics of polyurethane foam from waste refrigerators. *Waste Management & Research*. Epub ahead of print 10 October 2019. DOI: 10.1177/0734242X19877682.

Yin L, Fei L, Cui F, et al. (2007) Superporous hydrogels containing poly (acrylic acid-co-acrylamide)/O-carboxymethyl chitosan interpenetrating polymer networks. *Biomaterials* 28: 1258–1266.

Yu S, Su W, Wu D, et al. (2019) Thermal treatment of flame retardant plastics: A case study on a waste TV plastic shell sample. *Science of The Total Environment* 675: 651–657.

Zeng X, Mathews JA and Li J (2018) Urban mining of e-waste is becoming more cost-effective than virgin mining. *Environmental Science & Technology* 52: 4835–4841.

Zhao C, Zhang X and Shi L (2017) Catalytic pyrolysis characteristics of scrap printed circuit boards by TG-FTIR. *Waste Management* 61: 354–361.